



Cite this: *Phys. Chem. Chem. Phys.*,
2017, **19**, 29305

Photodissociation dynamics of fulvenallene and the fulvenallenyl radical at 248 and 193 nm[†]

Isaac A. Ramphal,^{ab} Mark Shapero,^{ab} Courtney Haibach-Morris^b and Daniel M. Neumark^{ab*}

Photofragment translational spectroscopy was used to study the photodissociation of fulvenallene, C₇H₆, and the fulvenallenyl radical, C₇H₅, at 248 nm and 193 nm. Starting from fulvenallene, only the H-atom loss channel producing the fulvenallenyl radical, C₇H₅, was observed. Fulvenallene dissociation occurs on the ground state surface with no exit barrier, and there is good agreement between our experimentally determined photofragment translational energy distribution and a prior distribution for a statistical process. Subsequent absorption at both wavelengths by fulvenallenyl enabled investigation of the photodissociation of this radical. Two channels were observed: C₅H₃ + C₂H₂ and C₄H₂ + C₃H₃. The photofragment translational energy distributions for these channels are peaked away from 0 kcal mol⁻¹, which is consistent with ground state dissociation over an exit barrier. At 248 nm, the C₃H₃-loss channel accounted for 85 ± 10% of fulvenallenyl dissociation, while at 193 nm it accounted for 80 ± 15%. The experimental branching between these channels is in reasonable agreement with Rice–Ramsperger–Kassel–Marcus theory calculations, which predict C₃H₃-loss to account for 70% and 63% of dissociation for 248 nm and 193 nm respectively.

Received 11th August 2017,
Accepted 17th October 2017

DOI: 10.1039/c7cp05490d

rsc.li/pccp

1. Introduction

Fulvenallene is the global minimum of the C₇H₆ potential energy surface (PES)¹ and plays a key role in the combustion chemistry of aromatic compounds.^{2,3} It has been detected in large quantities in toluene flames by photoionization mass spectrometry.^{2,4} Shock tube experiments have identified H-atom loss to produce a C₇H₆ product as the most important thermal decomposition reaction for the benzyl radical.^{5,6} Fulvenallene is also the primary 248 nm photodissociation product of the benzyl radical.⁷ Hence, elucidation of the unimolecular dissociation pathways of fulvenallene is of considerable interest. To this end, we investigate the ultraviolet photodissociation dynamics of both fulvenallene and its primary photodissociation product, the fulvenallenyl radical (Fig. 1).

Fulvenallene was first observed and isolated by flash vacuum pyrolysis of suitable precursors.^{8,9} Its infrared and microwave spectra have been reported,^{10,11} and its gas phase and condensed phase chemistry has been investigated.^{12–15} Photoelectron spectroscopy^{16,17} and, more recently, photoionization

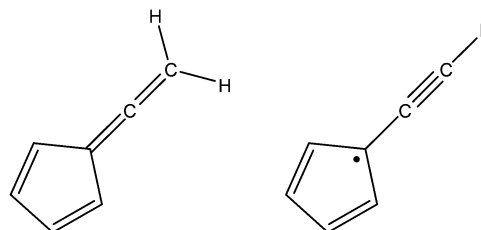
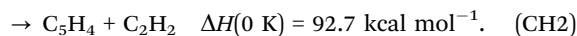
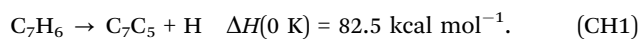


Fig. 1 Structures of fulvenallene and the fulvenallenyl radical.

mass spectrometry¹⁸ find the ionization potential (IP) of fulvenallene to be 8.22 eV.

Theoretical investigations of fulvenallene decomposition have found the following two lowest energy channels:¹⁹



Channel (1) corresponds to loss of an allenic H-atom and production of the resonance-stabilized fulvenallenyl radical; it proceeds through a loose transition state with no exit barrier. Channel (2) involves an intersystem crossing from the singlet to the triplet state, followed by dissociation over an exit barrier to yield cyclopentadienylidene and acetylene. A simplified C₇H₆ PES is shown in Fig. S1 of the ESI.[†] Calculations have suggested that decomposition *via* channel (2) following intersystem

^a Chemical Sciences Division, Lawrence Berkeley National Laboratory, Berkeley, California 94720, USA. E-mail: dneumark@berkeley.edu; Tel: +1-510-642-3502

^b Department of Chemistry, University of California, Berkeley, California 94720, USA

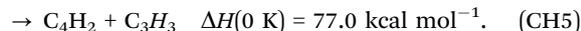
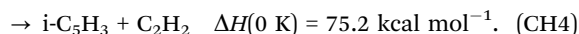
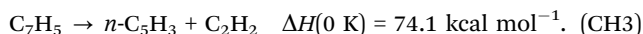
[†] Electronic supplementary information (ESI) available. See DOI: 10.1039/c7cp05490d

crossing to the triplet state occurs with comparable probability to H-atom loss.¹⁹

Velocity-map imaging experiments on the H-atom product of fulvenallene photodissociation (channel (1)) in the 245–255 nm energy range (assigned to the $D^1A_1 \leftarrow X^1A_1$ transition) were conducted by Giegerich and Fischer.²⁰ The H atoms were produced with a translational energy distribution peaked close to 0 kcal mol⁻¹, and with no dependence on excitation laser polarization. These results supported statistical and isotropic photodissociation dynamics subsequent to internal conversion to the electronic ground state. This work postulated that there must be a low probability of intersystem crossing in order to account for the large H-atom signal measured in these experiments. No attempts to measure channel (2) have been reported.

The fulvenallenyl radical product from channel (1) is greatly stabilized by electron delocalization over the cyclopentadienyl and propargyl moieties and is the global minimum of the C₇H₅ PES.²¹ Fulvenallenyl was detected experimentally by Steinbauer *et al.*¹⁸ by flash pyrolysis of a suitable precursor followed by photoionization mass spectrometry. Additionally, the IP of fulvenallenyl was found to be 8.19 eV using threshold photoelectron spectroscopy. An electronic absorption spectrum of the fulvenallenyl radical in a cryogenic Ne matrix has recently been reported, with an absorption band at 401 nm attributed to the origin of the $A^2B_1 \leftarrow X^2B_1$ transition.²² The present study considers transitions at energies much higher than in any previous reports.

Theoretical investigations of the C₇H₅ PES predict the following as the lowest energy decomposition channels:²³



In addition, several H-atom loss channels exist with $\Delta H(0 \text{ K}) > 90 \text{ kcal mol}^{-1}$. A simplified C₇H₅ PES is shown in Fig. S2 of the ESI.† There are multiple pathways to the products of channels (3)–(5), with a minimum of two isomerization steps prior to dissociation in each case. There are exit barriers for each of these channels, ~13–22 kcal mol⁻¹ for channel (3), ~15–17 kcal mol⁻¹ for channel (4), and ~8–10 kcal mol⁻¹ for channel (5). The dissociation products of channels (3)–(5) and their subsequent recombination processes have important implications for terrestrial combustion processes, as well as atmospheric photochemistry and molecular weight growth in the outer planets and their moon systems.^{2,24–30}

The flash pyrolysis/photoionization experiments in which fulvenallenyl was observed yielded smaller mass fragments as well;¹⁸ subsequent work proposed that these originated from fulvenallenyl dissociation *via* channels (3)–(5) in the pyrolysis source.³¹ A detailed combustion kinetics model^{2,3} based on theoretical work^{19,21,32,33} produced good agreement with the concentration *vs.* temperature profiles of the species in channels (1)–(5) that were produced from toluene in combustion flow reactors and detected by photoionization mass spectrometry. The importance of these models to understanding the

combustion of aromatic hydrocarbons demands closer inspection of the constituent reactions.

As the previous study of fulvenallene photodissociation was only sensitive to H-atoms, and because such studies on the fulvenallenyl radical are non-existent, we investigated the ultraviolet photodissociation dynamics of both of these species *via* molecular beam photofragment translational spectroscopy at 248 nm and 193 nm. In principle, all reaction products of channels (1)–(5) can be detected by this technique.

For fulvenallene photodissociation at both wavelengths, we only observe evidence for channel (1). The fulvenallenyl photoproduct from this channel then absorbs another photon, and evidence for channels (3)–(5) is observed for the radical photodissociation. Each process is consistent with a statistical mechanism on the ground electronic state, with dissociation occurring directly for channel (1) from fulvenallene, and over exit barriers for channels (3)–(5) from the fulvenallenyl radical. These assignments are based on consideration of the experimental product translational energy distributions and their comparison to results from statistical theories of reactivity.

II. Experimental

Fulvenallene synthesis

Fulvenallene was produced *via* flash vacuum thermolysis of homophthalic anhydride vapor at the surface of a resistively heated wire.^{15,34} The product of the reaction was isolated as a yellow crystalline solid in a liquid N₂ cold trap, warmed to 0 °C, and transferred to an evacuated cylinder (usually 3–5 Torr) that was then filled to 3000 Torr with Ar or He. NMR spectroscopy confirmed the successful production of fulvenallene, ¹H-NMR (400 MHz, C₆D₆, Me₄Si): δ (ppm) 4.75 (2H, s, =CH₂), 6.27 (2H, m, *meta*-CH), 6.47 (2H, m, *ortho*-CH). The NMR data match spectra reported previously.¹⁵

A typical mass spectrum of fulvenallene measured in our instrument is provided in Fig. S3 of the ESI,† and shows good agreement with a previously reported electron impact ionization mass spectrum.⁸ The IP of $m/z = 90$ was determined by measurement of an electron impact ionization efficiency curve (IEC) as reported previously.⁷ The appearance potential of 8.3 eV determined using this technique closely matches the previously measured adiabatic IP of 8.22 eV.¹⁸

Photodissociation experiments

Photodissociation studies of fulvenallene and the fulvenallenyl radical were carried out on a modified crossed molecular beam apparatus with a fixed source and rotatable detector as described previously.^{35–37} A pulsed molecular beam of fulvenallene in a noble gas carrier was produced by supersonic expansion through the orifice of a piezoelectric valve. The molecular beam was collimated *via* passage through two skimmers. A retractable, slotted chopper wheel enabled characterization of the beam velocity, typically 1700 m s⁻¹ in He and 600 m s⁻¹ in Ar carrier gas; typical speed ratios, *i.e.* the ratio of the beam velocity to velocity spread, were found to be 12–18. The molecular beam was

crossed orthogonally with a focused, unpolarized laser pulse from a Lambda Physik LPX 200i excimer laser at either 248 nm or 193 nm. Operation of the laser at half the 200 Hz repetition rate of the pulsed valve allowed for shot-to-shot subtraction of the background signal.

Photofragments were collected as a function of laboratory scattering angle, Θ_{LAB} , in the plane defined by the laser and molecular beam. An electron impact ionizer nested within three differentially pumped regions and operated at 80 eV produced cations that were mass selected by a quadrupole filter and detected with a Daly style ion detector.^{38,39} The additional capability to tune the electron energy to as low as 4 eV enabled measurement of IECs.⁷ A multichannel scalar collected and binned ion signal as a function of arrival time to produce time-of-flight (TOF) spectra.

Center-of-mass translational energy distributions, $P(E_T)$, were determined *via* a forward convolution method in the PHOTRAN program,⁴⁰ whereby TOF spectra are simulated using a trial $P(E_T)$ that is iteratively adjusted until agreement with all experimental TOF spectra is reached. In the case of secondary photodissociation of primary photoproducts, the trial distribution is additionally convoluted over the primary photodissociation $P(E_T)$ in the CMLAB2 program⁴¹ to obtain the simulated TOF spectra.

Computational methods

Electronic structure. Optimized geometries were calculated at the B3LYP/6-31G++(d,p) level implemented in Gaussian 09.⁴² Time-dependent density functional theory (TD-DFT) using this functional and basis set were used to calculate electronic excited state energies and oscillator strengths of fulvenallene and the fulvenallenyl radical, as shown in Table S1 (ESI[†]). For these excited state properties the current TD-DFT method and functional produces good agreement with more sophisticated EOM-CCSD calculations, which themselves agree well with experimental results.^{43,44}

RRKM kinetics. Isomerization and dissociation kinetics were calculated using the full C_7H_5 surface developed by da Silva and Trevitt.²³ All dissociation and isomerization pathways on this surface involve passage over barriers that we treat as tight transition states. Stationary point energies and vibrational modes calculated by da Silva and Trevitt using G3SX B3LYP/6-31G(2df,p) were used, with internal rotational modes treated as hindered rotors.

Unimolecular rate constants for reactions across this surface were calculated using Rice–Ramsperger–Kassel–Marcus (RRKM) theory.^{45–47} The RRKM rate constant is given by

$$k(E) = \sigma \frac{W^\ddagger(E - E_0)}{h\rho(E)} \quad (1)$$

where σ is the reaction path degeneracy,⁴⁸ $W^\ddagger(E - E_0)$ is the sum of states of the transition state, h is the Planck constant, and $\rho(E)$ is the rovibrational density of states of the reactant at energy E . The steady-state approximation is applied to the concentration of intermediates, and the product channels (3)–(5) and the H-loss channels are treated as sinks. Ratios of asymptotic product concentrations give branching in the statistical limit

among the various product channels. The RRKM calculations were done using code written by the authors.

III. Results

All TOF experimental data are shown normalized by on-axis $m/z = 90$ signal intensity (per 1000 counts) and then scaled to counts per 10^6 laser shots. Spectra with low signal are further scaled for comparison purposes as specified on an individual basis. Based on the known energetics, the maximum laboratory frame scattering angles Θ_{LAB} for the heavy photofragment from fulvenallene dissociation channels (1) and (2) under different experimental conditions are shown in Table 1.

Fulvenallene photodissociation

For photodissociation of fulvenallene seeded in an Ar beam, $m/z = 89$ (C_7H_5^+) TOF spectra were measured at laboratory scattering angles from 3° up to 12° at 248 nm and up to 15° at 193 nm. No signal was observed at higher scattering angles. Fig. 2 and 3 show representative TOF spectra collected at 4° and 10° with laser fluences of $\Phi_{248\text{nm}} = 25 \text{ mJ cm}^{-2}$ per pulse and $\Phi_{193\text{nm}} = 300 \text{ mJ cm}^{-2}$ per pulse respectively. The higher fluence at 193 nm was necessitated by considerably lower signal levels at that wavelength, reflecting the lower oscillator strength (Table S1, ESI[†]). Data collected for very long scans at lower

Table 1 Heavy photofragment maximum scattering angles for fulvenallene photodissociation channels (1) and (2) for different excitation wavelengths and carrier gases. The C_2H_2 -loss photoproducts are not constrained when Ar is the carrier

Channel	Maximum Θ_{LAB}	
	He	Ar
H-Loss		
248 nm	6	18
193 nm	9	26
C_2H_2 -Loss		
248 nm	34	—
193 nm	61	—

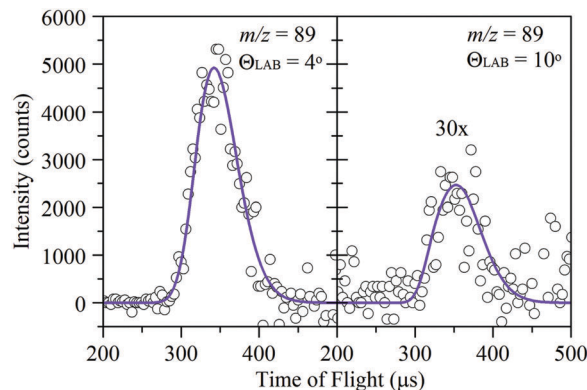


Fig. 2 TOF spectra for $m/z = 89$ at $\Theta_{\text{LAB}} = 4^\circ$ and 10° ($\Phi_{248\text{nm}} = 25 \text{ mJ cm}^{-2}$). The solid line simulations are generated using the experimental H-atom loss $P(E_T)$ in Fig. 8.

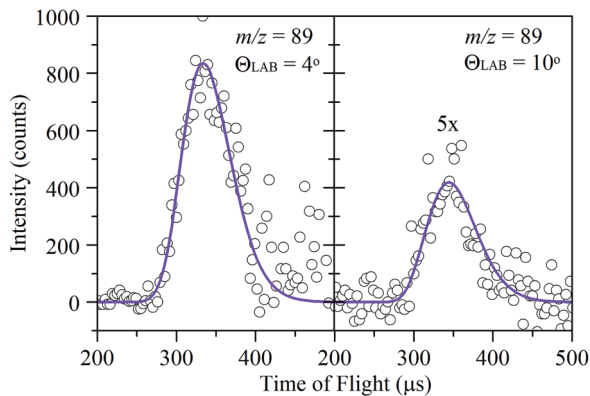


Fig. 3 TOF spectra for $m/z = 89$ at $\theta_{\text{LAB}} = 4^\circ$ and 10° ($\Phi_{193\text{nm}} = 300 \text{ mJ cm}^{-2}$). The solid line simulations are generated using the experimental H-atom loss $P(E_\gamma)$ in Fig. 8.

fluence, $\Phi_{193\text{nm}} = 50 \text{ mJ cm}^{-2}$, do not present any deviations from the data included here. All spectra in Fig. 2 and 3 comprise a single peak.

The H-atom counter-fragment for this dissociation channel cannot be detected due to its short residence time in the ionizer and extremely large Newton sphere, coupled with high background signal at $m/z = 1$. No evidence for the predicted cyclopentadienylidene + acetylene dissociation products of channel (2) is observed.¹⁹

Primary photofragment characterization

The large signal at $m/z = 89$ enables physical characterization of this primary photofragment. Fig. 4 shows IECs for $m/z = 89$ along the molecular beam axis with no photodissociation, as well as 4° away from the molecular beam axis with the 248 nm dissociation laser turned on. Along the molecular beam axis, the IEC intercepts the energy axis at 12.1 eV and $m/z = 89$ signal is attributed to dissociative ionization (DI) of fulvenallene in the ionizer. When the IEC for $m/z = 89$ is collected at $\theta_{\text{LAB}} = 4^\circ$, the appearance potential shifts to

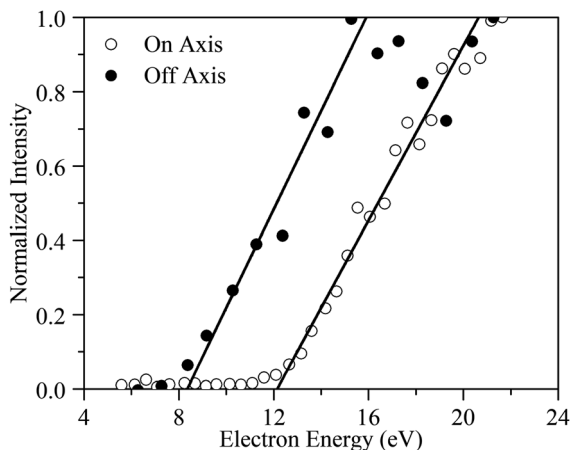


Fig. 4 Ionization efficiency curves for $m/z = 89$ taken along the molecular beam axis with the laser off (\circ) and 4° off the molecular beam axis with the laser on (\bullet). On axis the appearance potential is 12.1 eV, whereas off axis it is 8.4 eV.

8.4 eV, in acceptable agreement with the experimentally measured value of 8.19 eV for the adiabatic IP of the fulvenallenyl radical.¹⁸ The fragmentation pattern of the $m/z = 89$ radical is shown in Fig. S4 of the ESI.† This spectrum was collected by measuring TOF spectra at $\theta_{\text{LAB}} = 5^\circ$ with m/z values covering all possible combinations of up to seven C atoms and five H atoms, using an electron impact ionization energy of 80 eV. The signal for each spectrum was normalized by the $m/z = 89$ signal at 5° that was continually remeasured throughout the experiment.

At 248 nm, there is insufficient internal energy following dissociation to allow for isomerization to other C_7H_5 isomers on the reported PES.²³ The next lowest energy isomer lies $38.7 \text{ kcal mol}^{-1}$ above fulvenallenyl (12, Fig. S2, ESI†), while $E_{\text{avail}} = 33 \text{ kcal mol}^{-1}$ at 248 nm. Although isomerization is possible at 193 nm ($E_{\text{avail}} = 66 \text{ kcal mol}^{-1}$), C_7H_5 molecules with enough translational energy to scatter into $\theta_{\text{LAB}} > 3^\circ$ will have insufficient internal energy to surmount the $64.5 \text{ kcal mol}^{-1}$ isomerization barrier, and we report only data collected at $\theta_{\text{LAB}} \geq 4^\circ$. These considerations further support our assertion that the $m/z = 89$ signal should be attributed solely to the fulvenallenyl radical.

Evidence for secondary photodissociation

While studying fulvenallene photodissociation, there initially seemed to be evidence for acetylene-loss *via* channel (2). This channel should produce signal at $m/z = 64$ (C_5H_4^+) and $m/z = 26$ (C_2H_2^+), and there was extremely weak signal observed at $m/z = 64$ (C_5H_4^+) up to 30° . The $m/z = 26$ (C_2H_2^+) fragment was observed over the full $\sim 45^\circ$ angular range accessible by our apparatus. However, the observed counts for $m/z = 64$ were consistent with the expected ^{13}C isotope ratio for C_5H_3 based on counts for this species at $m/z = 63$, and the TOF spectra were identical. In addition, $m/z = 63$ (C_5H_3^+) was observed at LAB angles as large as 40° in the experiment, which exceeds the maximum $\theta_{\text{LAB}} = 34^\circ$ for channel (2) following 248 nm photoexcitation of fulvenallene (see Table 1). These observations suggest that the signals at $m/z = 64$ and 63 do not arise from channel (2).

The TOF spectra for masses below $m/z = 64$ taken within the allowed angular range for H-atom loss from fulvenallene (Table 1) display at least two features that have different laser fluence dependence, as shown in Fig. 5. There is a fast feature apparent for both $m/z = 62$ (C_5H_2^+) and $m/z = 50$ (C_4H_2^+) at high laser fluence that disappears at lower laser fluence. The slower feature present at all laser fluences is due to DI of fulvenallenyl. If two dissociation channels were both active and caused by single-photon dissociation of fulvenallene, the relative intensity of both features would be independent of laser fluence. The differing fluence dependences for the two peaks suggests that the faster peak in the TOF spectra for $m/z < 64$ arises from secondary photodissociation of fulvenallenyl radicals that absorb a second photon after they are produced; a model showing that such a mechanism is consistent with the observed fluence dependences is discussed in more detail in the ESI.†

Fulvenallenyl photodissociation

Secondary photodissociation of the fulvenallenyl primary photofragment was studied at 248 and 193 nm at laser fluences

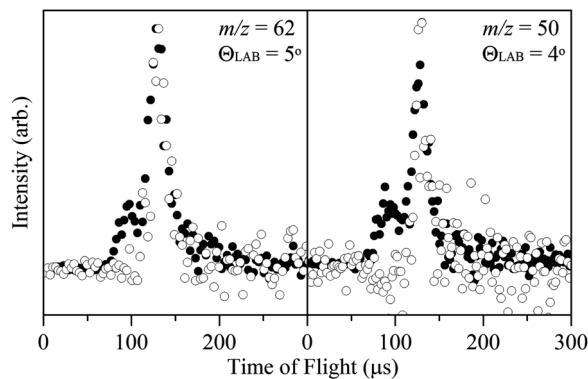


Fig. 5 Left panel: $m/z = 62$ at 330 mJ cm^{-2} (●) and 50 mJ cm^{-2} (○) per pulse at $\theta_{\text{LAB}} = 5^\circ$, right panel: $m/z = 50$ at 330 mJ cm^{-2} (●) and 25 mJ cm^{-2} (○) per pulse at $\theta_{\text{LAB}} = 4^\circ$. The 248 nm excimer is used for these measurements. These spectra are normalized to the slow, intense feature due to DI of the fulvenallenyl radical in the ionizer.

$\Phi_{248\text{nm}} = 420 \text{ mJ cm}^{-2}$ and $\Phi_{193\text{nm}} = 300 \text{ mJ cm}^{-2}$. These experiments were performed using He as the carrier gas. For channels (3)–(5), the Newton circles are such that the laboratory angular range over which scattering can occur is not kinematically constrained, in contrast to channel (1) for fulvenallene photodissociation.

Fig. 6 and 7 show TOF spectra collected for $m/z = 63$ (C_5H_3^+), $m/z = 50$ (C_4H_2^+), $m/z = 39$ (C_3H_3^+) and $m/z = 26$ (C_2H_2^+) at $\theta_{\text{LAB}} = 10^\circ$ for photoexcitation at 248 nm and 193 nm, respectively.

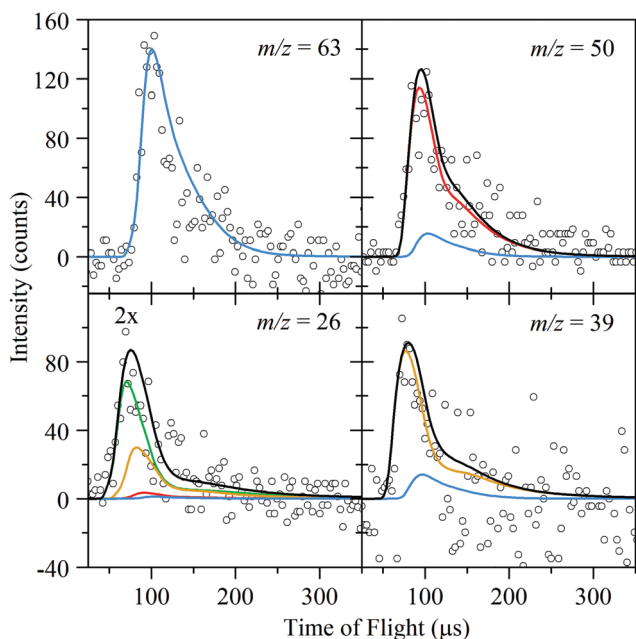


Fig. 6 TOF spectra for $m/z = 63$, $m/z = 50$, $m/z = 39$ and $m/z = 26$ at $\theta_{\text{LAB}} = 10^\circ$ at 248 nm ($\Phi_{248\text{nm}} = 420 \text{ mJ cm}^{-2}$). The blue ($m/z = 63$) and green ($m/z = 26$) simulations are generated using the $P(E_T)$ in Fig. 9a, while the red ($m/z = 50$) and yellow ($m/z = 39$) simulations are generated using the $P(E_T)$ in Fig. 9b. For TOF spectra with multiple features, the total simulation is shown in black. Note that DI of the three heavier fragments along with ionization of C_2H_2 contribute to the $m/z = 26$ TOF spectrum, as indicated by the presence of all four colors.

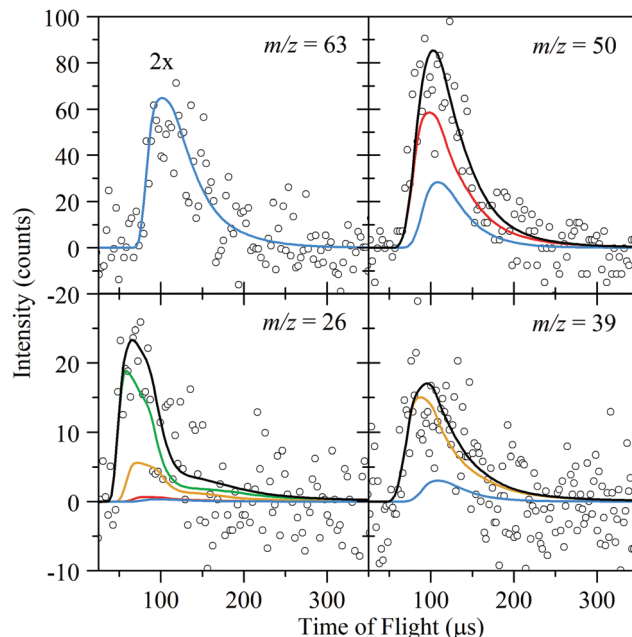


Fig. 7 TOF spectra for $m/z = 63$, $m/z = 50$, $m/z = 39$ and $m/z = 26$ at $\theta_{\text{LAB}} = 10^\circ$ at 193 nm ($\Phi_{193\text{nm}} = 300 \text{ mJ cm}^{-2}$). The blue ($m/z = 63$) and green ($m/z = 26$) simulations are generated using the $P(E_T)$ in Fig. 9c, while the red ($m/z = 50$) and yellow ($m/z = 39$) simulations are generated using the $P(E_T)$ in Fig. 9d. For TOF spectra with multiple features, the total simulation is shown in black.

These TOF spectra were collected beyond the Newton circles for H-loss from fulvenallene, and therefore do not contain the slow feature due to DI of the fulvenallenyl radical seen in Fig. 5. Additional TOF spectra at $\theta_{\text{LAB}} = 30^\circ$ are shown in Fig. S5, ESI†. These ion masses correspond to the parent fragments of the lowest energy dissociation pathways of the fulvenallenyl radical, channels (3)–(5). For both wavelengths, these features were observed over the full $\sim 45^\circ$ angular range accessible by our apparatus. Signal collected at $m/z = 88$ was entirely consistent with DI of fulvenallenyl, and no signal that could be attributed to the H-atom loss channels available to the fulvenallenyl radical was observed.

Beyond the Newton circles for fulvenallene H-atom loss, there is no dissociative ionization signal from the primary photofragment (fulvenallenyl), and thus no signal for $m/z > 64$. TOF spectra were collected at $m/z = 64, 63, 62, 61, 60, 52, 51, 50, 49, 48, 39, 38, 37, 36, 27, 26, 25, 24, 16, 15, 13$, and 12. It is not possible to measure signal at $m/z = 40, m/z = 28$ and $m/z = 14$ due to high argon and nitrogen background in the ionizer. These TOF spectra allow a construction of the fragmentation patterns of the mass 63 and mass 50 photofragments by normalizing the signal collected at each m/z value (Fig. S6 of the ESI†).

IV. Analysis

Primary photodissociation of fulvenallene

For each dissociation channel, the TOF spectra are governed by the center-of-mass (CM) angular and translational energy distribution, $P(E_T, \theta)$, which we assume are uncoupled to yield

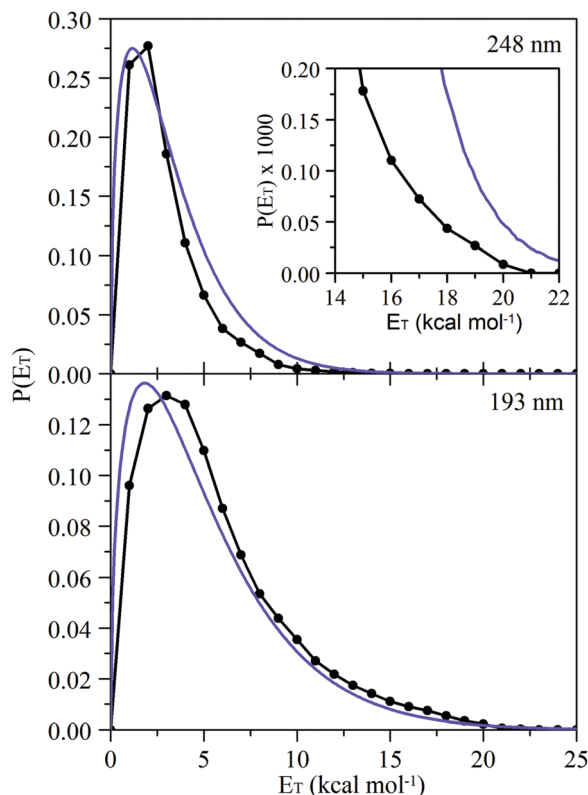


Fig. 8 The $P(E_T)$ distributions that best match experimental data (black) and one-photon prior distributions (purple) for fulvenallene H-atom loss following photoexcitation at 248 nm (top) and 193 nm (bottom). The tail at high E_T is necessary to adequately simulate all TOF spectra at 248 nm.

$$P(E_T, \theta) = P(E_T)I(\theta). \quad (2)$$

Here $P(E_T)$ is the CM translational energy distribution and $I(\theta)$ is the CM angular distribution. All TOF spectra can be adequately simulated by assuming isotropic angular distributions. For a given dissociation channel, conservation of linear momentum ensures both photofragments are simulated by the same $P(E_T)$ distribution.

At 248 nm, a fulvenallene molecule dissociating *via* H-loss channel (1) will have $E_{\text{avail}} = 33 \text{ kcal mol}^{-1}$ available for internal and translational energy partitioning. At 193 nm, $E_{\text{avail}} = 66 \text{ kcal mol}^{-1}$ for this channel. The $P(E_T)$ distributions that best simulate $m/z = 89$ (C_7H_5^+) TOF spectra at all observed laboratory angles are shown in Fig. 8. For these distributions, the peak translational energy, average translational energy $\langle E_T \rangle$, maximum translational energy $E_{T,\text{max}}$, and average fraction of the available energy that goes into product translation $\langle f_T \rangle$, are shown in Table 2. These characteristics for the $P(E_T)$ distribution measured by Giegerich and Fischer for the H-atom counter-fragment of this channel collected at 247 nm are also shown for comparison.²⁰

A statistical dissociation process with no exit barrier is expected to produce a $P(E_T)$ distribution similar to the prior distribution,⁴⁹ which has the analytical form

$$P(E_T) \propto E_T^{-1/2} \rho_{\text{vib}}(E_{\text{avail}} - E_T). \quad (3)$$

In eqn (3), ρ_{vib} is the vibrational density of states evaluated as a function of $E_{\text{avail}} - E_T$, where E_{avail} is the difference between the

Table 2 Characteristics of the $P(E_T)$ distributions in Fig. 8 determined for C_7H_5 , and the 247 nm $P(E_T)$ for H measured by Giegerich and Fischer.²⁰ At 248 nm and 193 nm, $E_{\text{avail}} = 33 \text{ kcal mol}^{-1}$ and 66 kcal mol^{-1} respectively

Fragment	Peak (kcal mol^{-1})	$\langle E_T \rangle$ (kcal mol^{-1})	$E_{T,\text{max}}$ (kcal mol^{-1})	$\langle f_T \rangle$
248 nm				
C_7H_5	1.5	2.9	21	0.09
H ^a	1.2	3.2	23	0.09
prior	1.2	3.2	—	0.09
193 nm				
C_7H_5	3.1	5.6	22	0.09
prior	1.8	5.1	—	0.08

^a Data from ref. 20.

absorbed photon energy and the activation barrier for the reaction, and E_T is the translational energy of the fulvenallenyl product.⁴⁹ There is reasonable agreement both at 248 nm and 193 nm between the $P(E_T)$ that best simulates the experimental TOF spectra and their respective single-photon prior distributions shown in Fig. 8.

Secondary photodissociation of the fulvenallenyl radical

Fulvenallenyl radicals that absorb a second photon will have sufficient energy to undergo secondary photodissociation. These radicals are produced with a distribution of internal energies determined by the $P(E_T)$ distributions for H-atom loss from fulvenallene (Fig. 8). In order to obtain the correct $P(E_T)$ distributions for the secondary photodissociation of fulvenallenyl, it is necessary to convolute the secondary $P(E_T)$ distributions over these primary H-loss distributions, which can be done in the analysis program CMLAB2. Fulvenallenyl dissociation *via* channels (3) + (4) gives rise to parent ion signals at $m/z = 63$ (C_5H_3^+) and $m/z = 26$ (C_2H_2^+), while channel (5) produces parent ion signals at $m/z = 50$ (C_4H_2^+) and $m/z = 39$ (C_3H_3^+). Conservation of linear momentum requires the two fragments from each channel to be simulated by the same $P(E_T)$. This condition is satisfied for the $P(E_T)$ distributions shown in Fig. 9a–d; the characteristics of these distributions are listed in Table 3. We now describe the fitting procedure in more detail.

As the heaviest secondary photofragment, the $m/z = 63$ (C_5H_3^+) TOF spectra can be used to construct the full $P(E_T)$ for the fulvenallenyl $\rightarrow \text{C}_5\text{H}_3 + \text{C}_2\text{H}_2$ channel without having to contend with DI signal from other fragments. As such, the $m/z = 63$ (C_5H_3^+) TOF spectra shown in Fig. 6 and 7 are adequately simulated using only contributions from the $m/z = 63$ (C_5H_3^+) secondary photoproduct, *i.e.* the $P(E_T)$ distributions in Fig. 9a and c.

The $m/z = 50$ (C_4H_2^+) and $m/z = 39$ (C_3H_3^+) TOF spectra shown in Fig. 6 and 7 differ significantly from the simulation produced for DI of $m/z = 63$ (C_5H_3^+), which does not adequately simulate the fast edge of the peak. Agreement with the experimental $m/z = 50$ (C_4H_2^+) TOF spectra requires simulations including contributions from the $m/z = 50$ (C_4H_2^+) photofragment of channel (5), as well as DI from $m/z = 63$ (C_5H_3^+). Simulation of the $m/z = 39$ (C_3H_3^+) TOF spectra include

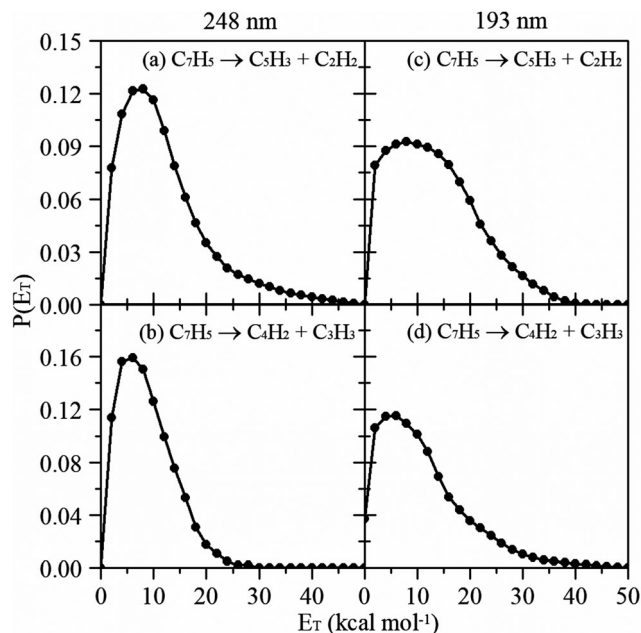


Fig. 9 Center-of-mass $P(E_T)$ distributions for secondary photodissociation of the fulvenallenyl radical at 248 nm (left) and 193 nm (right) to produce $C_5H_3 + C_2H_2$ (top) and $C_4H_2 + C_3H_3$ (bottom).

Table 3 Characteristics of the $P(E_T)$ distributions in Fig. 9

Channel	Peak (kcal mol ⁻¹)	$\langle E_T \rangle$ (kcal mol ⁻¹)	$E_{T,max}$ (kcal mol ⁻¹)	E_{avail} (kcal mol ⁻¹)	$\langle f_T \rangle$
248 nm					
C_2H_2 loss	7.0	12.1	48	74	0.16
C_3H_3 loss	6.0	9.1	28	71	0.13
193 nm					
C_2H_2 loss	8.0	13.3	42	139	0.10
C_3H_3 loss	5.0	11.3	48	137	0.08

contributions from the momentum-matched propargyl counter-fragment for channel (5), as well as DI signal from $m/z = 63$ ($C_5H_3^+$).

Construction of the $P(E_T)$ for $C_4H_2 + C_3H_3$ is complicated by the fact that the parent ions and all DI fragments produced by either of these photofragments are also formed by DI of $m/z = 63$ ($C_5H_3^+$). The $P(E_T)$ distributions for this channel (Fig. 9b and d) are constructed by finding the distribution that best simulated $m/z = 50$ ($C_4H_2^+$) and $m/z = 39$ ($C_3H_3^+$) signal across the entire angular range, and which all have a consistent weighting of the $m/z = 63$ ($C_5H_3^+$) contribution.

The TOF spectra for $m/z = 26$ ($C_2H_2^+$) are simulated using a contribution from the momentum-matched acetylene counter-fragment for the $C_5H_3 + C_2H_2$ dissociation channel, Fig. 9a and c, as well as DI signal from the $m/z = 63$ ($C_5H_3^+$), $m/z = 50$ ($C_4H_2^+$), and $m/z = 39$ ($C_3H_3^+$) fragments. Given that all other photofragments dissociatively ionize to $m/z = 26$ ($C_2H_2^+$), the weighting of each contribution to these TOF spectra are calculated using the product branching ratio (details below). The major contributor to these TOF spectra is the parent ion from the acetylene photofragment produced through channels (3) + (4).

The experimental branching ratio (BR) between channel (5) and channels (3) + (4) can be calculated according to

$$BR\left(\frac{CH(3+4)}{CH(5)}\right) = \frac{W_{CH(3+4)} \sigma_{CH(5)} f_{CH(5)}}{W_{CH(5)} \sigma_{CH(3+4)} f_{CH(3+4)}} \quad (4)$$

In eqn (4), W_i is the weighted fraction of the $P(E_T)$ of channel i used to simulate the experimental spectra, σ_i is the ionization cross-section of the species i , calculated according to Fitch and Sauter,⁵⁰ and f_i is the relative fraction of the m/z value in the mass spectrum of the parent species.

To obtain f_i requires a mass spectrum for each photofragment used for the BR calculation. The fragmentation pattern collected off-axis (see Fig. S6, ESI[†]) was used for the C_5H_3 photofragment, while previously reported mass spectra^{51,52} were used for C_4H_2 . The fragmentation pattern collected off-axis for the mass 50 photofragment (Fig. S6, ESI[†]) is in excellent agreement with the mass spectrum for diacetylene. For C_3H_3 , we used the fragmentation pattern for scattered products from allene photodissociation at 193 nm (see Fig. S7, ESI[†]), since the dominant channel is H-atom loss to produce propargyl radicals.⁵³ The experimental data indicate that C_3H_3 -loss (channel (5)) accounts for $85 \pm 10\%$ and $80 \pm 15\%$ of fulvenallenyl decomposition at 248 nm and 193 nm respectively. The uncertainty in these branching ratios comes from the different weightings that can be used to adequately simulate the $m/z = 50$ and $m/z = 39$ TOF spectra.

The branching ratio calculated using eqn (4) can be compared with the results given by an RRKM calculation that represents the statistically expected branching ratio. Such a calculation requires consideration of the internal energy remaining in the primary photofragment. The fulvenallenyl radical internal energy is taken into account by integrating the RRKM analysis over the primary $P(E_T)$ distributions. The RRKM analysis predicts that C_3H_3 -loss accounts for 70% and 63% of fulvenallenyl decomposition at 248 nm and 193 nm respectively. The RRKM predictions are in reasonable agreement with the experimentally determined branching ratio between the C_3H_3 -loss and C_2H_2 -loss channels. The experimental and theoretical branching ratios display the same qualitative trend in which the contribution from C_2H_2 -loss increases slightly for higher excitation energy.

The RRKM calculations also predict that the combined H-atom loss channels accessible to the fulvenallenyl radical are negligible (<1% of dissociation) at both wavelengths used in this study. For the two acetylene-loss channels, the n - C_5H_3 isomer is calculated to account for 53% and 46% of the C_5H_3 signal at 248 nm and 193 nm respectively.

V. Discussion

This experiment was aimed at elucidating the primary photodissociation channels of fulvenallene at 248 and 193 nm. During the course of these investigations, it became clear that some of the fulvenallenyl radical produced from fulvenallene absorbs an additional photon and subsequently dissociates. In

this section, the dynamics of the primary and secondary dissociation channels are considered in more detail.

The fulvenallene H-atom loss channel was previously measured by Giegerich and Fischer.²⁰ The characteristics of the $P(E_T)$ that best simulates all of our 248 nm C_7H_5 TOF data are in excellent agreement with their study (Table 2) in which the H-atom counter-fragment was detected, with both distributions peaking close to 0 kcal mol⁻¹.²⁰ Our experimental $P(E_T)$ also compares reasonably well to a prior distribution for an idealized statistical ground state process. It is therefore likely that this channel proceeds *via* internal conversion to the ground electronic state, followed by intramolecular vibrational redistribution of the photon energy and then dissociation, consistent with the mechanism proposed by Giegerich and Fischer. While no previous work has been done on the photodissociation of fulvenallene at 193 nm, the dynamics appear to be similar to 248 nm in occurring through a statistical ground state mechanism. The lack of evidence for acetylene-loss from fulvenallene suggests a low probability for intersystem crossing¹⁹ relative to H-atom loss.

The C_7H_5 photoproduct from fulvenallene dissociation was identified as the fulvenallenyl radical based on agreement with the previously measured ionization potential.¹⁸ Measurements by Giegerich and Fischer give a ~ 100 ns lifetime for fulvenallenyl formation, with counts rising to 70% of their maximum value within the 30 ns duration of our laser pulse,²⁰ and the lifetime should be even shorter at 193 nm. It is therefore likely that nascent fulvenallenyl is formed in time to absorb a second photon. The experimentally observed laser fluence dependence of the $m/z = 89$ signal agrees quite well with a consecutive two-photon dissociation reaction (see the ESI†). This is consistent with the interpretation that the fulvenallenyl radical undergoes secondary photodissociation following absorption of a second ultraviolet photon.

The only previous study on the UV photophysics of the fulvenallenyl radical probed electronic transitions down to 365 nm.²² The present study demonstrates that absorption also occurs at 248 nm and 193 nm. Theoretical work on the C_7H_5 surface identified the lowest energy dissociation pathways of acetylene-loss (+i/*n*- C_5H_3) and propargyl-loss (+ C_4H_2), along with several higher energy H-atom loss channels.²³ Both of the heavy fragment channels were observed in this study, with no evidence for H-atom loss. The unimportance of H-atom loss and the dominance of propargyl-loss are consistent with the RRKM branching ratios and with previous theoretical investigations.³¹ The diacetylene photoproduct is specifically identified by the excellent agreement between the mass spectrum constructed from data collected off-axis for the $m/z = 50$ fragment and its dissociative ionization (Fig. S6, ESI†) and previously reported mass spectra for this species.^{51,52}

Production of i- C_5H_3 and *n*- C_5H_3 isomers from channels (3) and (4) is expected, but these isomers cannot be distinguished due to their similar IP values of 8.28 eV and 8.19 eV, respectively,⁵⁴ and because of the similar energetics of their dissociation. Previous calculations³¹ show higher concentrations of the *n*- C_5H_3 isomer over a large temperature and pressure range, whereas the RRKM analysis conducted here finds each isomer to be of

comparable importance. The fragmentation pattern constructed for the $m/z = 63$ fragment from data collected off-axis (Fig. S6, ESI†) shows significant differences from a previously measured mass spectrum for *n*- C_5H_3 .⁵⁵ While most the same mass fragments appear in the two mass spectra, the relative intensities of the peak clusters around the parent ion mass and $m/z = 50$ are reversed. This discrepancy may reflect production of appreciable amounts of both i- C_5H_3 and *n*- C_5H_3 during fulvenallenyl photodissociation, which is consistent with the RRKM prediction. In calculating the product channel branching ratios, the ionization cross sections of these two isomers are weighted according to their RRKM branching.

At both 248 nm and 193 nm, the distributions for the two secondary photodissociation channels peak away from 0 kcal mol⁻¹. The characteristics of these distributions are consistent with internal conversion to the ground state followed by statistical dissociation over an exit barrier. The $P(E_T)$ distributions for 193 nm secondary photodissociation are much broader and peak at slightly higher energies than at 248 nm, in line with expectations for higher E_{avail} . There is only a modest decrease in $\langle f_T \rangle$ with the much higher E_{avail} conferred by two 193 nm photons. At both dissociation wavelengths, the peak and average positions of these distributions are in line with calculated exit barrier heights of ~ 16 – 17 kcal mol⁻¹ for C_2H_2 -loss and ~ 8 – 10 kcal mol⁻¹ for C_3H_3 -loss (there are multiple pathways to each of these dissociation channels),²³ since one generally expects only part of the exit barrier height to be channeled into product translation.⁵⁶ In addition, the $P(E_T)$ distribution for channel (5), which is predicted to have the smaller exit barrier, peaks at lower E_T than for channels (3) + (4).

The general agreement between the RRKM and experimentally determined product branching ratios supports the assignment of statistical dissociation mechanisms for the product channels. The statistical nature of the dissociation reactions studied here leads to product branching ratios that agree reasonably well with those calculated by da Silva *et al.* for thermal decomposition of fulvenallenyl.³¹

VI. Conclusion

Fulvenallene photodissociates exclusively *via* H-atom loss following 248 nm and 193 nm photoexcitation to produce the fulvenallenyl radical, $C_7H_6 \rightarrow C_7H_5 + H$. The analysis of the TOF spectra supports internal conversion to the ground state followed by statistical dissociation. The lack of signal corresponding to the cyclopentadienylidene + acetylene dissociation channel demonstrates that the probability of intersystem crossing is low.

Secondary photodissociation of the primary fulvenallenyl photofragment occurs at both wavelengths and results in at least two dissociation channels: acetylene-loss to produce a C_5H_3 radical (i- and *n*-isomers both predicted), $C_7H_5 \rightarrow C_5H_3 + C_2H_2$; and propargyl radical loss to produce diacetylene, $C_7H_5 \rightarrow C_4H_2 + C_3H_3$. Based on the consistency between the

$P(E_T)$ distributions for these channels and the calculated exit barrier heights, and the reasonable agreement between the experimental branching ratios with those calculated using RRKM theory, it appears that the photodissociation of fulvenallenyl proceeds by internal conversion followed by ground state statistical dissociation for the radical. The predicted H-atom loss channels at much higher energy were not observed, and do not appear to play a meaningful role in the dissociation dynamics of the fulvenallenyl radical.

The dissociation channels reported here encompass the most important unimolecular photochemistry for fulvenallene and the fulvenallenyl radical. The statistical nature of these reactions suggests they are also the most important unimolecular thermal decomposition reactions for these species.

Conflicts of interest

There are no conflicts to declare.

Acknowledgements

This work was supported by the Director, Office of Basic Energy Sciences, Chemical Sciences, Geosciences, and Bioscience division of the U. S. Department of Energy under Contract DE-AC02-05CH11231. The authors would like to thank Preston Scrape and Laurie Butler for providing the CMLAB2 software used for part of the data analysis. This work was made possible in part thanks to contributions from the Eric B. Abramson Graduate Fellowship and the Klaus and Mary Ann Saegebarth Fellowship.

References

- 1 D. Polino, A. Famulari and C. Cavallotti, *J. Phys. Chem. A*, 2011, **115**, 7928–7936.
- 2 W. H. Yuan, Y. Y. Li, P. Dagaut, J. Z. Yang and F. Qi, *Combust. Flame*, 2015, **162**, 3–21.
- 3 W. H. Yuan, Y. Y. Li, P. Dagaut, J. Z. Yang and F. Qi, *Combust. Flame*, 2015, **162**, 22–40.
- 4 T. C. Zhang, L. D. Zhang, X. Hong, K. W. Zhang, F. Qi, C. K. Law, T. H. Ye, P. H. Zhao and Y. L. Chen, *Combust. Flame*, 2009, **156**, 2071–2083.
- 5 M. Braun-Unkhoff, P. Frank and T. Just, *Ber. Bunsenges. Phys. Chem.*, 1990, **94**, 1417–1425.
- 6 M. A. Oehlschlaeger, D. F. Davidson and R. K. Hanson, *J. Phys. Chem. A*, 2006, **110**, 6649–6653.
- 7 M. Shapero, N. C. Cole-Filipiak, C. Haibach-Morris and D. M. Neumark, *J. Phys. Chem. A*, 2015, **119**, 12349–12356.
- 8 E. Hedaya and M. E. Kent, *J. Am. Chem. Soc.*, 1970, **92**, 2149–2151.
- 9 P. Schissel, M. E. Kent, D. J. McAdoo and E. Hedaya, *J. Am. Chem. Soc.*, 1970, **92**, 2147–2149.
- 10 C. L. Angell, *J. Mol. Struct.*, 1971, **10**, 265–273.
- 11 T. Sakaizumi, F. Katoh, O. Ohashi and I. Yamaguchi, *J. Mol. Spectrosc.*, 1993, **159**, 112–121.
- 12 C. Wentrup, E. Wentrup-Byrne and P. Muller, *J. Chem. Soc., Chem. Commun.*, 1977, 210–211.
- 13 H. J. Lindner and K. Hafner, *Mol. Cryst. Liq. Cryst. Sci. Technol., Sect. A*, 1996, **276**, 339–348.
- 14 K. Hafner, *Pure Appl. Chem.*, 1990, **62**, 531–540.
- 15 J. Thapa, M. Spencer, N. G. Akhmedov and F. Goulay, *J. Phys. Chem. Lett.*, 2015, **6**, 4997–5001.
- 16 R. Botter, J. Jullien, J. M. Pechine, J. J. Piade and D. Solgadi, *J. Electron Spectrosc. Relat. Phenom.*, 1978, **13**, 141–143.
- 17 C. Müller, A. Schweig, W. Thiel, W. Grahn, R. G. Bergman and K. P. C. Vollhardt, *J. Am. Chem. Soc.*, 1979, **101**, 5579–5581.
- 18 M. Steinbauer, P. Hemberger, I. Fischer and A. Bodi, *ChemPhysChem*, 2011, **12**, 1795–1797.
- 19 D. Polino and C. Cavallotti, *J. Phys. Chem. A*, 2011, **115**, 10281–10289.
- 20 J. Giegerich and I. Fischer, *Phys. Chem. Chem. Phys.*, 2013, **15**, 13162–13168.
- 21 G. da Silva and J. W. Bozzelli, *J. Phys. Chem. A*, 2009, **113**, 12045–12048.
- 22 A. Chakraborty, J. Fulara and J. P. Maier, *Angew. Chem., Int. Ed. Engl.*, 2016, **55**, 228–231.
- 23 G. da Silva and A. J. Trevitt, *Phys. Chem. Chem. Phys.*, 2011, **13**, 8940–8952.
- 24 T. S. Zwier and M. Allen, *Icarus*, 1996, **123**, 578–583.
- 25 A. S. Wong, Y. L. Yung and A. J. Friedson, *Geophys. Res. Lett.*, 2003, **30**, 1447–1450.
- 26 P. P. Lavvas, A. Coustenis and I. M. Vardavas, *Planet. Space Sci.*, 2008, **56**, 67–99.
- 27 V. S. Meadows, G. Orton, M. Line, M. C. Liang, Y. L. Yung, J. Van Cleve and M. J. Burgdorf, *Icarus*, 2008, **197**, 585–589.
- 28 A. Maranzana, A. Indarto, G. Ghigo and G. Tonachini, *Combust. Flame*, 2013, **160**, 2333–2342.
- 29 G. da Silva, *J. Phys. Chem. A*, 2014, **118**, 3967–3972.
- 30 L. Zhao, Y. Tang, R. I. Kaiser, T. P. Troy, B. Xu, M. Ahmed, J. Alarcon, D. Belisario-Lara, A. M. Mebel, Y. Zhang, C. Cao and J. Zou, *Phys. Chem. Chem. Phys.*, 2017, **19**, 15780–15807.
- 31 G. da Silva, A. J. Trevitt, M. Steinbauer and P. Hemberger, *Chem. Phys. Lett.*, 2011, **517**, 144–148.
- 32 G. da Silva, J. A. Cole and J. W. Bozzelli, *J. Phys. Chem. A*, 2010, **114**, 2275–2283.
- 33 M. Derudi, D. Polino and C. Cavallotti, *Phys. Chem. Chem. Phys.*, 2011, **13**, 21308–21318.
- 34 R. J. Spangler and J. H. Kim, *Tetrahedron Lett.*, 1972, **13**, 1249–1251.
- 35 Y. T. Lee, J. D. McDonald, P. R. Lebreton and D. R. Herschbach, *Rev. Sci. Instrum.*, 1969, **40**, 1402–1408.
- 36 B. Negru, S. J. Goncher, A. L. Brunsvold, G. M. P. Just, D. Park and D. M. Neumark, *J. Chem. Phys.*, 2010, **133**, 074302.
- 37 B. Negru, G. M. P. Just, D. Park and D. M. Neumark, *Phys. Chem. Chem. Phys.*, 2011, **13**, 8180–8185.
- 38 N. R. Daly, *Rev. Sci. Instrum.*, 1960, **31**, 264–267.
- 39 K. Kuhnke, K. Kern, R. David and G. Comsa, *Rev. Sci. Instrum.*, 1994, **65**, 3458–3465.
- 40 S. A. Harich, *Photran*, 2003.

- 41 CMLAB2, version 6/93, modified by J. D. Myers. This is an interactive version built on the original cmlab2 program: Zhao, X. PhD Dissertation, University of California, 1988.
- 42 M. J. Frisch, G. W. Trucks, H. B. Schlegel, G. E. Scuseria, M. A. Robb, J. R. Cheeseman, G. Scalmani, V. Barone, B. Mennucci, G. A. Petersson, H. Nakatsuji, M. Caricato, X. Li, H. P. Hratchian, A. F. Izmaylov, J. Bloino, G. Zheng, J. L. Sonnenberg, M. Hada, M. Ehara, K. Toyota, R. Fukuda, J. Hasegawa, M. Ishida, T. Nakajima, Y. Honda, O. Kitao, H. Nakai, T. Vreven, J. A. Montgomery Jr., J. E. Peralta, F. Ogliaro, M. J. Bearpark, J. Heyd, E. N. Brothers, K. N. Kudin, V. N. Staroverov, R. Kobayashi, J. Normand, K. Raghavachari, A. P. Rendell, J. C. Burant, S. S. Iyengar, J. Tomasi, M. Cossi, N. Rega, N. J. Millam, M. Klene, J. E. Knox, J. B. Cross, V. Bakken, C. Adamo, J. Jaramillo, R. Gomperts, R. E. Stratmann, O. Yazyev, A. J. Austin, R. Cammi, C. Pomelli, J. W. Ochterski, R. L. Martin, K. Morokuma, V. G. Zakrzewski, G. A. Voth, P. Salvador, J. J. Dannenberg, S. Dapprich, A. D. Daniels, Ö. Farkas, J. B. Foresman, J. V. Ortiz, J. Cioslowski and D. J. Fox, *Gaussian 09*, Gaussian, Inc., Wallingford, CT, USA, 2009.
- 43 M. Caricato, G. W. Trucks, M. J. Frisch and K. B. Wiberg, *J. Chem. Theory Comput.*, 2011, 7, 456–466.
- 44 M. Miura, Y. Aoki and B. Champagne, *J. Chem. Phys.*, 2007, 127, 084103.
- 45 R. A. Marcus and O. K. Rice, *J. Phys. Chem.*, 1951, 55, 894–908.
- 46 T. Beyer and D. F. Swinehart, *Commun. ACM*, 1973, 16, 379.
- 47 D. C. Astholz, J. Troe and W. Wieters, *J. Chem. Phys.*, 1979, 70, 5107–5116.
- 48 A. J. Karas, R. G. Gilbert and M. A. Collins, *Chem. Phys. Lett.*, 1992, 193, 181–184.
- 49 R. D. Levine and R. B. Bernstein, *Acc. Chem. Res.*, 1974, 7, 393–400.
- 50 W. L. Fitch and A. D. Sauter, *Anal. Chem.*, 1983, 55, 832–835.
- 51 Z. M. Zhou and W. Z. Xue, *J. Organomet. Chem.*, 2009, 694, 599–603.
- 52 S. E. Stein, Director, NIST Mass Spec Data Center, “Mass Spectra”, in *NIST Chemistry WebBook, NIST Standard Reference Database Number 69*, ed. P. J. Linstrom and W. G. Mallard, National Institute of Standards and Technology, Gaithersburg MD, <http://webbook.nist.gov>, retrieved January 11, 2017, p. 20899.
- 53 J. C. Robinson, N. E. Sveum, S. J. Goncher and D. M. Neumark, *Mol. Phys.*, 2005, 103, 1765–1783.
- 54 B. Yang, C. Q. Huang, L. X. Wei, J. Wang, L. S. Sheng, Y. W. Zhang, F. Qi, W. X. Zheng and W. K. Li, *Chem. Phys. Lett.*, 2006, 423, 321–326.
- 55 X. B. Gu, Y. Guo and R. I. Kaiser, *Int. J. Mass Spectrom.*, 2007, 261, 100–107.
- 56 S. Kato and K. Morokuma, *J. Chem. Phys.*, 1980, 73, 3900–3914.